Research Square

Preprints are preliminary reports that have not undergone peer review.
They should not be considered conclusive, used to inform clinical practice,
or referenced by the media as validated information.

Universal Aspects of Shear Flow of Unentangled Polymer Melts

Manfred H. Wagner

manfred.wagner@tu-berlin.de

Berlin Institute of Technology (TU Berlin)

Research Article

Keywords: Single Integral Constitutive Equation, Doi-Edwards Equation, Rouse Relaxation Time Spectrum, Shear Viscosity, First and Second Normal Stress Difference, Universal Material Function

Posted Date: November 24th, 2026

DOI: https://doi.org/10.21203/rs.3.rs-11690773/v1

License: This work is licensed under a Creative Commons Attribution 4.0 International License.
Read Full License

Additional Declarations: No competing interests reported.

Rapid Communication

Universal Aspects of Shear Flow of Unentangled Polymer Melts

Manfred H. Wagner

Polymer Engineering/Polymer Physics, Berlin Institute of Technology (TU Berlin), Ernst-Reuter-Platz 1, 10587 Berlin, Germany

KEYWORDS: Single Integral Constitutive Equation, Doi-Edwards Equation, Rouse Relaxation Time Spectrum, Shear Viscosity, First and Second Normal Stress Difference, Universal Material Function

ABSTRACT

Shear viscosity and normal stress data reported by Dalne et al. [Macromolecules (2025) 58:7062-7083] for three unentangled polystyrene melts with molar mass of 10, 20, and 30kg/mol are analyzed based on the single integral constitutive equation approach developed by Poh et al. [Rheol. Acta (2020) 59:755–763]. Because the terminal relaxation regime relevant for flow properties of unentangled polymers is determined by an inseparable combination of (entropic) Rouse and (energetic) glassy modes, they proposed the use of a spectrum of effective Rouse modes encompassing both entropic and energetic relaxation effects and depending on two

parameters, modulus G and Rouse time τ_R, which are determined directly from steady-state shear flow data. Unentangled chains are oriented but not stretched in steady-state shear flow, and we show that shear viscosity as well as first and second normal stress difference predicted by the Doi-Edwards Independent Alignment (DEIA) model with a relaxation time spectrum of effective Rouse modes are in agreement with available experimental evidence. Normalized shear viscosity, normalized first and second normal stress coefficient, as well as the ratio of the second to the first normal stress difference are universal material functions of unentangled polymers independent of molar mass. In start-up of shear flow, chains are initially oriented and stretched, but the stretch relaxes in steady-state shearing. Without introducing any new parameter, the transient shear viscosity can be described by the Rotation Zero Stretch (RZS) model of Wagner et al. [Rheol. Acta (2024) 63:573–584], which reduces to the DEIA model in steady-state shear flow.

1. INTRODUCTION

The recently reported shear flow data of Dalne et al. (2025) on transient and steady shear flow of three polystyrene (PS) melts PS10k, PS20k, and PS30k with molar masses of (nominally) 10, 20 and 30kg/mol have sparked renewed interest in the rheology of unentangled polymers. Early shear viscosity data of Stratton (1972) for two PS melts with molar mass of 10.5 kg/mol and 19.8 kg/mol as well as later transient shear viscosity and first normal stress data of Santangelo and Roland (2001) for a PS melt with molar mass of 13kg/mol were limited in scope, but provided sufficient evidence of shear-thinning of unentangled melts with a scaling of $\dot{\gamma}^{-1/2}$ in the limit of high shear rates $\dot{\gamma}$. By using rotational rheometry with cone-partitioned plate (CPP) fixtures, Dalne et al. (2025) not only presented transient shear viscosity characterization of the three PS melts considered, but also reported the (steady-state) first normal stress difference N_1 and, for the first time, also the second normal stress difference N_2 of unentangled melts as a function of shear rate. Surprisingly, the shear rheology of unentangled polymer melts resembles that of entangled polymer melts and shows transient shear viscosity overshoot, shear thinning of viscosity and normal stress coefficients, a negative second normal stress difference, and a slightly decreasing ratio $\beta = -N_1/N_2$ with increasing shear rate from approximately $\beta = 0.3$ *to* 0.1. We do not discuss the experimental measurement details in this short contribution, but refer to Dalne et al. (2025) and references therein.

The shear data of Santangelo and Roland (2001) were modeled by Ianniruberto and Marrucci (2020) using Brownian dynamics simulation of Fraenkel chains representing the Rouse modes. They assumed flow-induced reduction of the monomeric friction coefficient and fitted the functional expression of the monomeric friction coefficient to the steady-state viscosity data. A similar approach was applied by Psevdos and Ianniruberto (2026) to the data set of Dalne et al.

(2025). The authors concluded that (contrary to data) single-chain simulations predict a zero second normal stress difference, suggesting the presence of many-chain effects other than only flow-induced friction reduction. Dalne et al. (2025) themselves presented a new molecular picture for unentangled melts, based on the Rouse model and the concept of tension blobs [Colby et al. 2007], which was later expanded by Parisi and coworkers (2021) to the "shear slit" model. The highly elaborate and extensive modeling based on this picture is in agreement with the shear viscosity data, while the scaling of the first normal stress difference disagrees strongly with the experimental data.

Both the modeling of Ianniruberto and coworkers as well as of Dalne and coworkers relied on linear-viscoelastic (LVE) mastercurves of storage and loss modulus and the linear superposition of Rouse relaxation modes and glassy modes, despite the fact of thermorheological complexity and the breakdown of time-temperature superposition (TTS) in the vicinity of the glass transition temperature T_g. It is well known that polymers exhibit distinct temperature dependences for segmental or α-relaxation and for terminal flow relaxation (Plazek 1965, Plazek and O'Rouke 1971, Nagai et al. 1987, Plazek and Nagai 1991, Plazek et al. 1993, Ngai and Plazek 1995, Santangelo and Roland 1998, Roland et al. 2001) with a stronger temperature dependence of the segmental relaxation compared to the terminal relaxation. This puts in question the validity of LVE mastercurves constructed by TTS. In addition, while according to Ngai and co-workers (Ngai, et al. 1997, Ngai and Plazek 2007, Ngai 2011) at temperatures sufficiently higher than T_g, the steady-state recoverable compliance J_s^0 of unentangled polymers is well predicted by the conventional Rouse model, J_s^0 decreases significantly as the test temperatures approaches T_g. This drop in recoverable compliance is even more accentuated in the case of low molar mass unentangled polymers. The glassy and Rouse modes cannot be separated in the vicinity of the

glass transition temperature because entropic elasticity is increasingly affected by energetic interactions. Nevertheless, shear-thinning of unentangled melts occurs with an exponent of -½ in the limit of high shear rates, which is the hallmark of Rouse relaxation. In view of this situation, Narimissa and Wagner (2020) and Poh et al. (2020) proposed the use of "effective" Rouse modes encompassing both entropic and energetic effects in the terminal regime. Using a single integral constitutive equation of the Doi-Edwards Independent Alignment (DEIA) type in combination with a Rouse relaxation time spectrum of effective Rouse modes, they showed agreement of model predictions with the shear viscosity as well as the first normal stress coefficient data of Santangelo and Roland (2001). The shear viscosity data of Stratton (1972) agree also quantitatively with the universal mastercurve predicted by Wagner and Narimissa (2020) for unentangled melts approaching a scaling of -½ at sufficiently high shear rates [Poh et al. 2020].

The intention of this short contribution is to analyze the steady and transient shear data reported by Dalne et al. (2025) using the single integral constitutive equation approach with effective Rouse modes developed by Poh et al. (2020), which is extended here to the Rotation Zero Stretch (RZS) model of Wagner et al. (2024). We compare model predictions to the transient and steady shear viscosity and the first and second normal stress difference, and assess the universality of shear flow of unentangled melts.

2. MATERIALS AND RHEOLOGICAL CHARACTIZATION

The molecular characteristics of the PS melts investigated by Dalne et al. (2025) are summarized in Table 1. The polydispersity index of the samples is reported as 1.02. The melts can be considered as unentangled because their molar mass M is less than the critical molar mass for entanglements, i.e., $M < M_c \cong 2M_e$, with $M_c = 31.2$kg/mol [Fetters et al. 2007].

Table 1. Molecular Characteristics of the Polystyrene Melts: Molar mass M, glass transition temperature T_g, steady-state compliance J_s^0 and $J_{s,R}^0$ at $T_{ref} = T_g + 15K$.

Sample	M (kg/mol)	T_g [°C]	J_s^0 [1/MPa]	$J_{s,R}^0$ [1/MPa]
PS10k	10.5	96.1	0.62	1.32
PS20k	19.3	101.5	1.87	2.38
PS30k	29.1	102.7	3.05	3.58

The linear and nonlinear rheometry was performed by an ARES rheometer (TA, USA) with parallel-pate fixture and CPP geometries, respectively. Details are given by Dalne et al. (2025). Figure 1 shows the linear-viscoelastic mastercurves of storage (G') and loss modulus (G'') as well as the tangent of the loss angle δ of the PS samples at the same distance from the glass transition temperature ($T_{ref} = T_g + 15K$) as reported by Costanzo (2026). As expected, the mastercurves superimpose at the glass transition, while showing increasing scatter with decreasing molar mass of the samples.

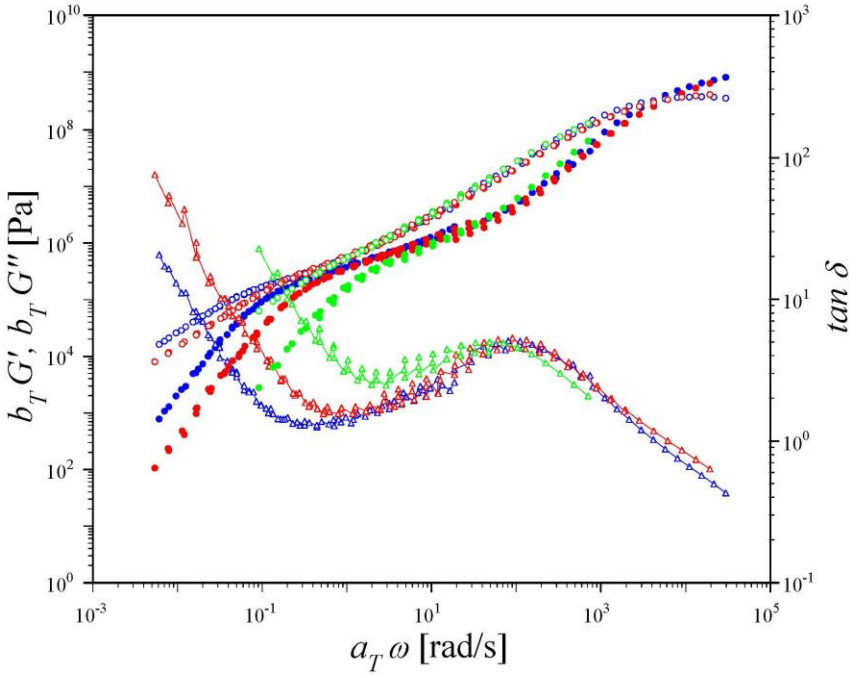

Fig.1: Storage modulus *G'*, loss modulus *G''*, and tangent of loss angle δ for PS10k (green), PS20k (red) and PS30k (blue) at $T_{ref} = T_g + 15K$.

A full linear-viscoelastic characterisation in the experimental frequency window can be obtained by using a parsimonious relaxation spectrum with

$$G(t) = \sum_i g_i \exp(-t/\tau_i) \qquad (1)$$

The partial moduli g_i and relaxation times τ_i were determined by the IRIS software [Winter and Mours 2006], and the steady-state compliance J_s^0 was calculated from

$$J_s^0 = \frac{\sum_i g_i \tau_i^2}{\eta_0^2} = \frac{\sum_i g_i \tau_i^2}{\left(\sum_i g_i \tau_i\right)^2} \qquad (2)$$

η_0 is the zero-shear viscosity.

On the other hand, the Rouse relaxation time spectrum is given by

$$G_R(t) = \sum_{i=1}^{n} G_i \exp(-i^2 t / \tau_R) \quad (3)$$

with the sum over all *n* Rouse modes of the chain. The moduli G_i are independent of index *i* with $G_i = G = \frac{\rho RT}{M}$ (4)

ρ is the density, *R* the molar gas constant and *T* the absolute temperature. In the limit of large *n*, the Rouse relaxation time τ_R and the steady-state compliance $J^0_{s,R}$ of the Rouse model are given by

$$\tau_R = \frac{6}{\pi^2}\frac{\eta_0}{G} \quad (5)$$

and

$$J^0_{s,R} = \frac{0.4}{G} = 0.4\frac{M}{\rho RT} \quad (6)$$

The values of J^0_s and $J^0_{s,R}$ at the reference temperature $T_{ref} = T_g + 15K$, i.e. at equal distance from the glass transition temperature are given in Table I. J^0_s decreases more than $J^0_{s,R}$ with decreasing molar mass, indicating the increasing effect of the glassy interaction on the Rouse modes in agreement with the expectations of Nagai (2011).

3. MODELLING APPROACH

Following Narimissa and Wagner (2020), we recall that as shown by Lodge and Wu (1971) the constitutive equation of the Rouse model is fully equivalent to the rubberlike-liquid equation,

$$\sigma(t) = \int_{-\infty}^{t} \frac{\partial G_R(t-t')}{\partial t'} \mathbf{C}^{-1}(t,t')dt' \tag{7}$$

$\sigma(t)$ is the extra stress tensor, and $\mathbf{C}^{-1}(t,t')$ the relative Finger strain tensor. At time *t'*, each Rouse mode is characterized by an isotropic distribution of normalized end-to-end vectors $\mathbf{u}(t')$. At the observation time *t*, the unit vectors $\mathbf{u}(t')$ are deformed to vectors $\mathbf{u}'(t,t')$. The Rouse model assumes affine deformation, and therefore by use of the relative deformation gradient tenor $\mathbf{F}^{-1}(t,t')$ we obtain

$$\mathbf{u}'(t,t') = \mathbf{F}^{-1}(t,t') \cdot \mathbf{u}(t') \tag{8}$$

The Finger strain tensor $\mathbf{C}^{-1}(t,t')$ is the average dyadic product

$$\mathbf{C}^{-1} = 3\langle \mathbf{u}'\mathbf{u}' \rangle \tag{9}$$

with the dependence on *t* and *t'* understood. The bracket denotes an average over an isotropic distribution of unit vectors $\mathbf{u}(t')$ and is obtained by a surface integral over the unit sphere,

$$\langle\ \rangle \equiv \frac{1}{4\pi} \oiint [\ ] \sin\theta\, d\theta\, d\varphi \tag{10}$$

In shear flow, the rubberlike-liquid equation results in a constant shear viscosity $\eta = \eta_0$, a constant first normal stress coefficient $\psi_1 = \psi_{10}$ and a zero second normal stress coefficient ψ_2. Using the Rouse relaxation time spectrum and in the limit of large *n* we obtain

$$\eta_0 = \frac{\pi^2}{6} G \tau_R \tag{11}$$

$$\psi_{10} = \frac{\pi^4}{45} G \tau_R^2 \tag{12}$$

$$\psi_{20} = 0 \tag{13}$$

In order to find a more realistic nonlinear viscoelastic constitutive equation, Poh et al. (2020) retained the linear-viscoelastic spectrum of the Rouse model but consider a different nonlinear strain measure. Instead of affine deformation, they assumed that strands are oriented, but not stretched. This is equivalent to the "affine rotation" assumption of the Doi-Edwards Independent Alignment (DEIA) model, which, by the same arguments as used by Doi and Edwards (1978), but replacing the relaxation modulus of the tube model by the Rouse relaxation modulus $G_R(t)$ of Eq.(3), results in

$$\sigma(t) = \int_{-\infty}^{t} \frac{\partial G_R(t-t')}{\partial t'} \mathbf{S}_{\mathbf{DE}}^{\mathbf{IA}}(t,t')dt' \tag{14}$$

The DEIA deformation tensor $\mathbf{S}_{\mathbf{DE}}^{\mathbf{IA}}$ is given by

$$\mathbf{S}_{\mathbf{DE}}^{\mathbf{IA}} = 5\,\mathbf{S} = 5\left\langle \frac{\mathbf{u}'\mathbf{u}'}{u'^2} \right\rangle \tag{15}$$

with $\mathbf{S}$ being the relative second order orientation tensor with the dependence on t and t' understood. The orientation tensor $\mathbf{S}$ requires a normalization factor of 5 in Eq.(15) instead of 3 as in Eq.(9). Poh et al. (2020) showed quantitative agreement of Eq.(14) with the shear viscosity data presented by Stratton (Stratton 1972) and Santangelo and Roland (2001). For later use we

note that Eq.(14) predicts a shear-rate dependent negative second normal stress difference N_2 with a normal stress coefficient ψ_{20} in the second order limit of

$$\psi_{20} = -\frac{2}{7}\psi_{10} \tag{16}$$

Wagner et al. (2024) extended the DEIA model for shear flow to the Rotation Zero Stretch (RZS) model, which we reformulate here by introducing the Rouse relaxation modulus,

$$\sigma(t) = G_R(t) f^2(t,t' \le 0)\mathbf{S}_{DE}^{IA}(t,t' \le 0) + \int_0^t \frac{\partial G_R(t-t')}{\partial t'}\mathbf{S}_{DE}^{IA}(t,t')dt' \tag{17}$$

The first term on the right hand side accounts for the contribution to the stress tensor of Rouse modes, which were created *before* the inception of flow, i.e. during the times $-\infty < t \le 0$, and have not yet relaxed at the time of observation at time *t*. They experience the stretch $f(t,t' = 0)$ and the orientation $\mathbf{S}_{DE}^{IA}(t,t'=0)$ between time $t' = 0$, when shear flow started, and the observation time *t*. The second (integral) term accounts for the stress contribution of Rouse modes, which were created at times *t' during* flow, i.e. in the time frame of $0 < t' \le t$. These entanglement strands do not experience stretch due to the rotational component of shear flow. Stretch is obtained from the evolution equation

$$\frac{\partial f(t,t' \le 0)}{\partial t} = f\left[\mathbf{K}(t) : \mathbf{S}(t,t' \le 0)\right] - \frac{(f^5 - 1)}{5\tau_R} \tag{18}$$

The first term of the right-hand side of Eq.(18) expresses affine deformation with **K** being the deformation rate tensor, and the second term Rouse stretch relaxation. For a frame-indifferent formation of the RZS model see Narimissa et al. (2020). Note that for small stretches f with $f - 1 << 1$, Eq.(18) reduces to the classical relation

$$\frac{\partial f}{\partial t} = f(\mathbf{K} : \mathbf{S}) - \frac{1}{\tau_R}(f - 1) \tag{19}$$

We also note that the RZS model consisting of Eqs.(18) and (19) converges to the steady-state stress tensor of the Doi-Edwards IA equation,

$$\sigma(t \to \infty) = \int_{-\infty}^{t \to \infty} \frac{\partial G_R(t-t')}{\partial t'} \mathbf{S}_{DE}^{IA}(t,t')dt' \tag{20}$$

4. COMPARISON BETWEEN MODEL PREDICTIONS AND DATA

4.1 Parameter identification

The RZS model relies on only 2 molecular parameters for linear **and** nonlinear rheology, the modulus G and the Rouse time τ_R. Because their determination from the terminal regime of the mastercurves of G' and G'' is questionable due to issues with TTS as discussed above, we follow Wagner and Narimissa (2020) by invoking effective Rouse modes directly fitted to the shear viscosity data. By doing so we make use of Eq.(11), which relates the zero-shear viscosity η_0 to the product of G and τ_R. Taking the experimentally determined value of η_0 from the start-up shear flow data, only either G or τ_R has to be fitted. (We remark that in principal G and τ_R could be determined univocally if in addition to η_0 reliable experimental data of ψ_{10} would be available as suggested by Poh et al. (2020).)

The zero-shear viscosities and the best-fit molecular parameters of PS10k, PS20k and PS30k at measurement temperature T_m are summarized in Table 2. Also given in Table 2 is the ratio φ of the modulus G of the effective Rouse modes to the theoretical modulus G_E according to Eq.(4), which assumes that the modulus of the Rouse chain would only depend on entropic elasticity,

$$\varphi = \frac{G}{G_E} = G\frac{M}{\rho RT} \tag{21}$$

As expected the energetic impact on the modulus G as expressed by φ is the larger the smaller the molar mass of the polymer.

Table 2. Rheological characteristics of the Polystyrene Melts: Measurement temperature T_m, Zero-shear viscosity η_0, Modulus G, Rouse time τ_R at T_m.

Sample	T_m (°C)	η_0 [kPa s]	G [kPa]	τ_R [s]	φ [-]
PS10k	115	310	780	0.24	2.54
PS20k	125	165	285	0.35	1.67
PS30k	130	135	165	0.50	1.43

By taking the effective Rouse spectrum with the parameters of PS30k at T_m=130°C as reference, and by shifting the effective spectra of PS10k and PS20k to this reference, we create mastercuves of *G'*, *G''* and *tan δ* of the effective Rouse modes for all three polymers considered as shown by the black lines in Figure 2. Also shown in Figure 2 are the experimental LVE data from Figure 1, shifted horizontally and vertically to fit the terminal regime of the effective Rouse modes. While superposition of the experimentally determined mastercurves in the vicinity of the glass transition is lost, superposition in the terminal regime is now achieved, confirming the existence of Rouse modes in the terminal regime. However, as expected the range of fit decreases with decreasing molar mass of the polymer due to the increasing impact of the glassy modes.

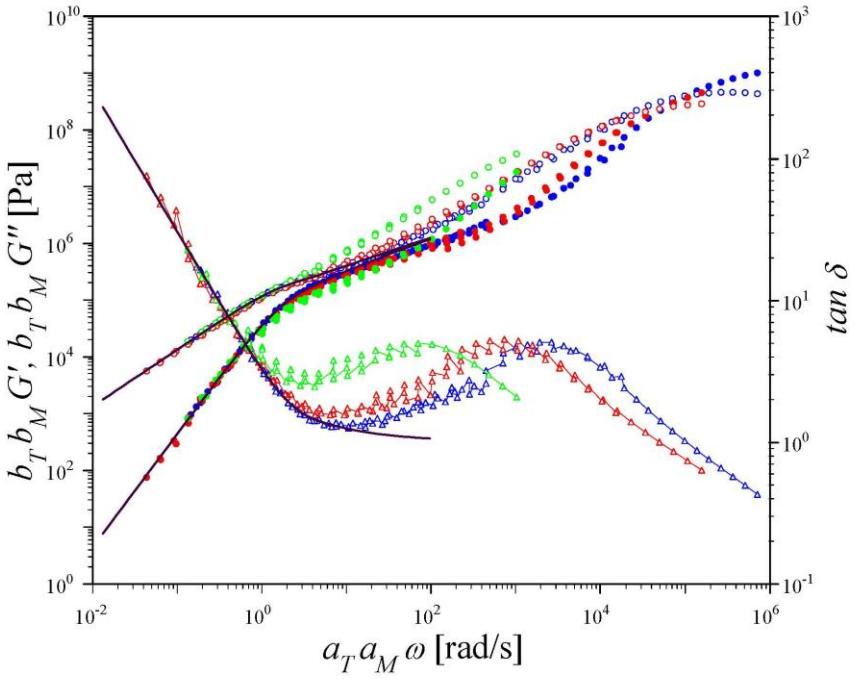

Fig.2: Shifted storage modulus *G'*, loss modulus *G''*, and tangent of loss angle δ for PS10k (green), PS20k (red) and PS30k (blue). Black lines are mastercurves of effective Rouse modes. For details see text.

Figure 3a shows the dependence of *G* on molar mass. Although we have only 3 data points, which, however, span the interesting range from 10 to 30kg/mol, the line in Fig.3a indicates clearly a slope of -3/2, instead of the expected slope of -1 from Eq.(4). The difference is made up by the factor φ defined by Eq.(21) and included in Table 2, which has a slope of -1/2 (Fig.3b). This means that the energetic impact of the glassy modes is inverse proportional to the square root of the molar mass and therefore inverse proportional to the radius of gyration of the chain. Shorter chains are more closely packed together leading to enhanced energetic intra-and inter-chain interactions. Extrapolating the line in Figure 3b to φ=1, we may say with all caution that the terminal relaxation

regime of (then entangled) polymers with molar masses of $M \geq 60kg/mol$ is no longer influenced by the effect of glassy modes.

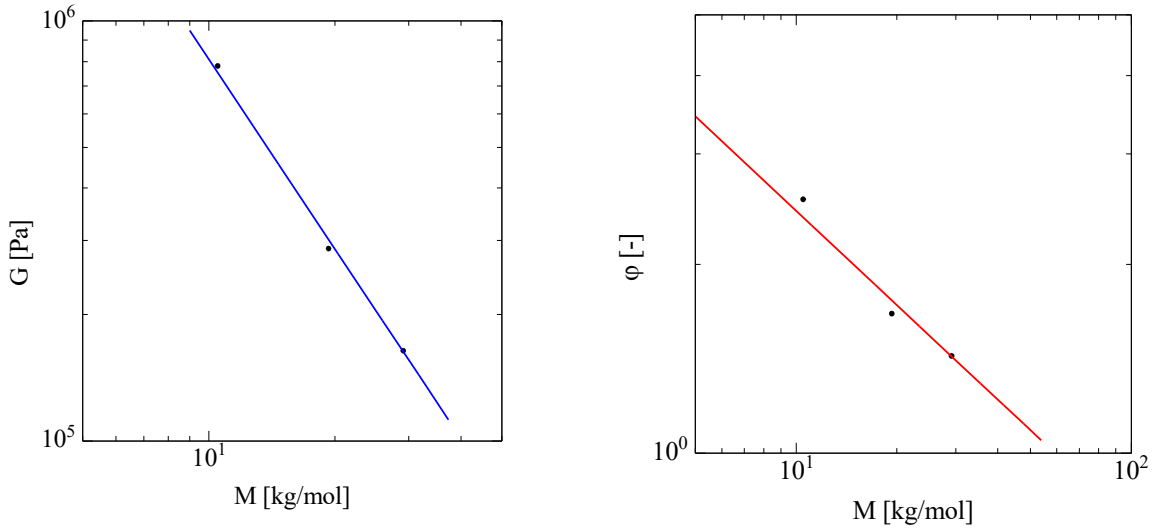

(a) (b)

Fig.3: (a) Modulus G of effective Rouse modes, and (b) factor φ as a function of molar mass M. Line in (a) indicates $G \propto M^{-3/2}$, line in (b) $\varphi \propto M^{-1/2}$.

4.2 Transient shear viscosity

Figure 4 shows the quality of the fit obtained by the RZS model of Eq.(17) for the transient shear viscosity $\eta^+(\dot{\gamma},t)$ and the transient shear stress $\sigma_{12}^+(\dot{\gamma},\gamma)$ of PS10k as a function of shearing time t and shear deformation γ at the measurement temperature T_m of 115°C. We recall that this is obtained by fitting only one molecular parameter (either G or τ_R) to the linear and nonlinear transient shear viscosity data.

For PS20k, the transient shear viscosity data at the lowest and highest shear rate show some uncertainty (Fig.5). Therefore G and τ_R are fitted to the (steady-state) shear viscosities of shear rates in the range of $1 \le \dot{\gamma} \le 20 s^{-1}$, resulting in a (calculated) zero-shear viscosity of $\eta_0 = 165\ Pa\ s$ from Eq.(11) at the measurement temperature T_m of 125°C. Figure 6 presents the transient shear viscosity $\eta^+(\dot{\gamma},t)$ and the transient shear stress $\sigma_{12}^+(\dot{\gamma},\gamma)$ of PS30k at the measurement temperature T_m of 130°C. In this case there is again only one fitting parameter (either G or τ_R) needed because the zero-shear viscosity η_0 is well captured experimentally.

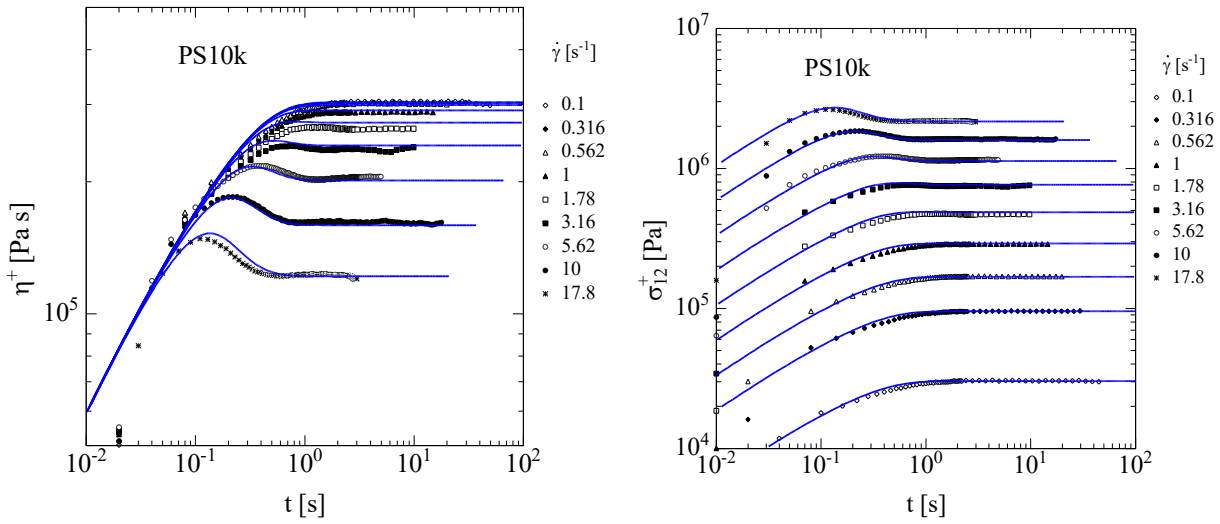

Fig.4: Transient shear viscosity $\eta^+(\dot{\gamma},t)$ and shear stress $\sigma_{12}^*(\dot{\gamma},\gamma)$ data (symbols) for PS10k at $T_m = 115°C$. Lines are predictions of the RZS model, Eq.(17).

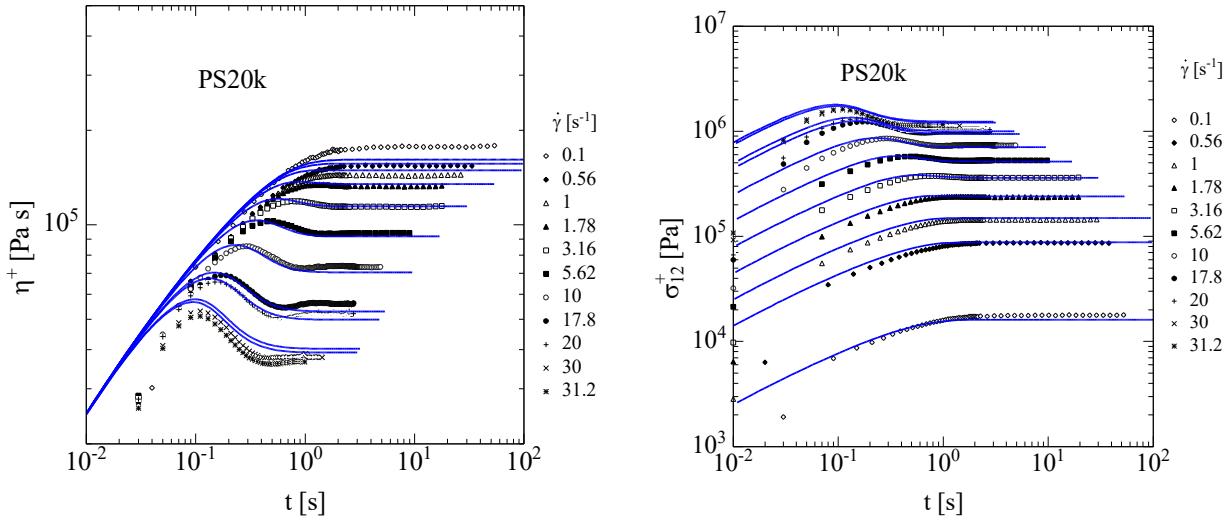

Fig.5: Transient shear viscosity $\eta^+(\dot{\gamma},t)$ and shear stress $\sigma_{12}^*(\dot{\gamma},\gamma)$ data (symbols) for PS20k at $T_m = 125°C$. Lines are predictions of the RZS model, Eq.(17).

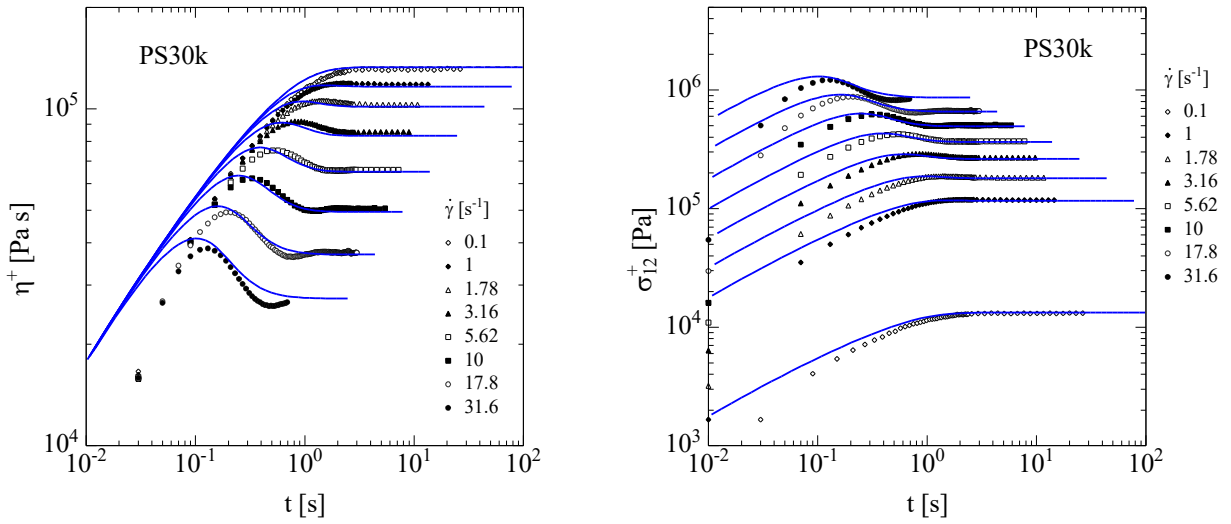

Fig.6: Transient shear viscosity $\eta^+(\dot\gamma,t)$ and shear stress $\sigma^*_{12}(\dot\gamma,\gamma)$ data (symbols) for PS30k at $T_m = 130°C$. Lines are predictions of the RZS model, Eq.(17).

The normalized shear viscosity as a function of Weissenberg number $Wi = \dot\gamma\tau_R$ is presented in Figure 7a. As already shown by Poh et al. (2020), the data are in agreement with the universal normalized viscosity function $\eta/\eta_0(Wi)$ derived from Eq.(20) and approach a scaling of $Wi \propto \dot\gamma^{-1/2}$ at higher Wi as shown by the dotted line. Also the maximal value of the shear viscosity at the overshoot, $\eta_{\max}$, normalized by the (steady-state) shear viscosity η and plotted in dependence of Wi is a universal function of the RZS model of Eq.(17). $\eta_{\max}/\eta$ increases with Wi according to $Wi \propto \dot\gamma^{0.14}$ as shown by the dotted line in Figure 7b. The shear deformation at the maximal shear viscosity, $\gamma_{\max}$, increases with Wi as shown in Figure 7c. However, the agreement of data and RZS model is only qualitative in this case, both showing an upward trend.

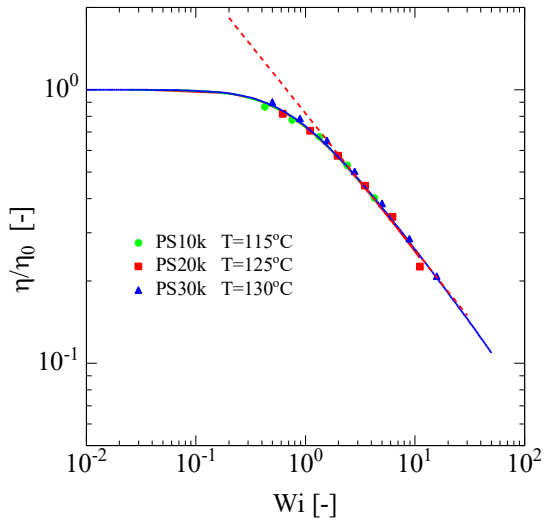

(a)

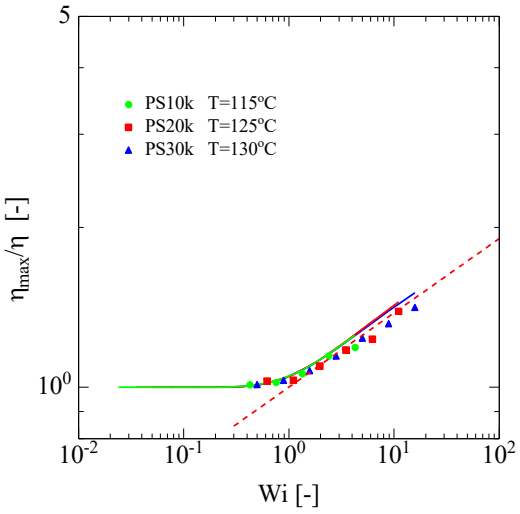

(b)

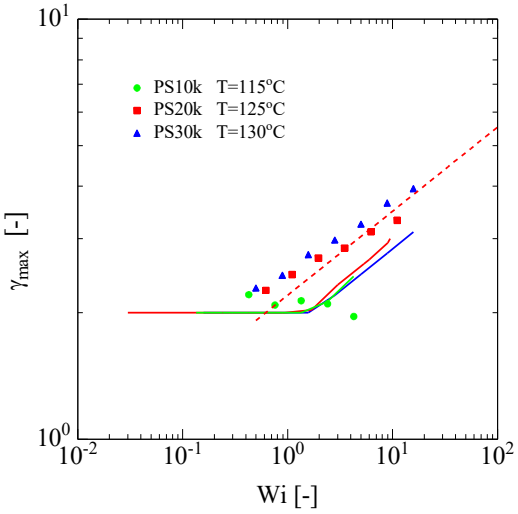

(c)

Fig.7: (a) Normalized shear viscosity η/η_0, (b) normalized maximal viscosity at the overshoot η_{max}/η, and (c) maximal shear deformation γ_{max} as a function of Weissenberg number $Wi = \dot{\gamma}\tau_R$. Full lines are predictions of the RZS model, Eq.(17). Dotted line in (a) indicates $\eta/\eta_0 \propto Wi^{-1/2}$, in (b) $\eta_{max}/\eta \propto Wi^{0.14}$, and (c) $\gamma_{max} \propto Wi^{0.2}$.

4.2 First and second normal stress difference

Normal stress difference data were reported by Dalne et al. (2025) for PS20k and PS30k. The data (symbols) of N_1 and N_2 and the corresponding normal stress coefficients (Costanzo 2026) are plotted in Figure 8 as a function of shear rate $\dot{\gamma}$. Agreement with predictions of the DEIA model of Eq.(20) (lines) is found for the first normal stress difference, and also the trend of the second normal stress difference data is well captured by the model, in spite of the considerable scatter due the difficulties involved in measuring N_2. We recall that this is achieved by only one (PS30k) or two molecular parameters defining the effective Rouse relaxation modes.

In order to investigate the scaling of the normal stress differences, we plot the normal stresses of PS30k for the extended shear rate range of $0.1 < \dot{\gamma} < 100 s^{-1}$ in Figure 9. The dotted line in Fig.9a with a slope of 2 represents the scaling expected in the second order regime for N_1, while the dotted line with a slope of ½ is the high shear rate scaling of the Rouse model. The same scaling is observed by N_2. Dalne et al. (2025) reported exponents of 1.14 for N_1 and 0.88 for N_2 for PS30k. The empirical exponents reported represent the transition from the small shear rate second order to the high shear rate regime taking place in the experimental window, with the transition occurring at smaller shear rates for N_2 than for N_1. This is shown in Figure 9b, where in addition to the high shear rate scaling of $\psi_1/\psi_{10} \propto \dot{\gamma}^{-3/2}$ (dotted line), also the ratio β of the (negative) second to the first normal stress coefficients, $\beta = -\psi_2/\psi_1$, is shown by the long-dashed curve. β has the value of 2/7 in the second order regime, Eq.(7), and approaches a constant value of β=1/7 at high shear rates, corresponding to the value for β obtained in step-shear strain relaxation for the Doi-Edwards (DE) model without the independent alignment assumption. The normalized normal stress coefficients ψ_1/ψ_{10} and ψ_2/ψ_{20} as well as β are

universal material functions of the DEIA model with the Rouse relaxation time spectrum, Eq.(20), if plotted as a function of $Wi = \dot{\gamma}\tau_R$. This is shown in Figure 10 for the case of $\beta(Wi)$ for the normal stress data of PS20k and PS30k. Within the large scatter caused mainly by the scatter of the second normal stress difference data, the experimental data for β of PS20k agree with those of PS30k and show a decreasing trend with increasing Wi in the experimentally investigated transition regime, in general agreement with the DEIA model of Eq.(20).

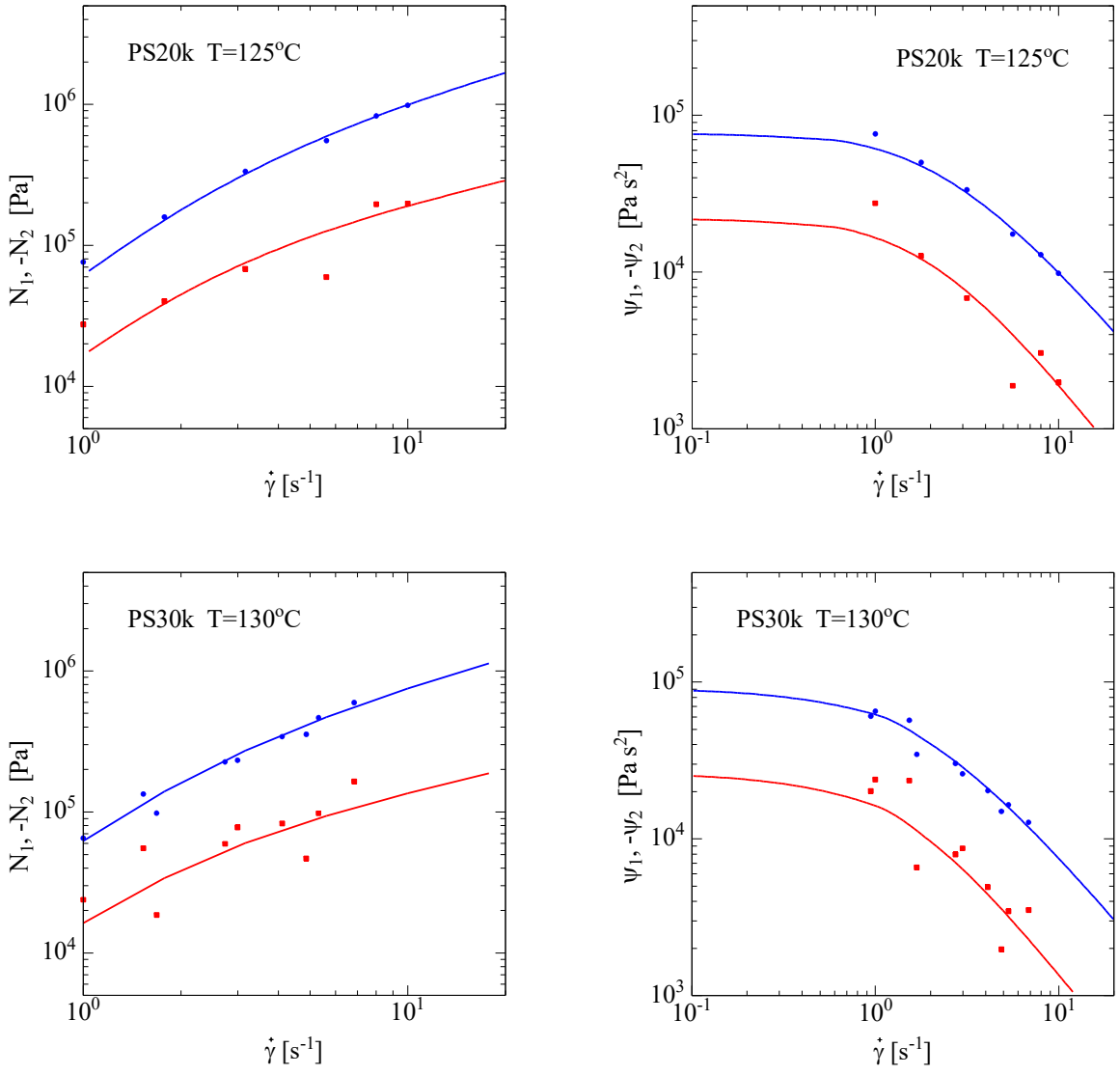

Fig.8: First and second normal stress difference and normal stress coefficient data (symbols) for PS20k and PS30k as a function of shear rate $\dot{\gamma}$. Lines are predictions of the DEIA model (Eq.(20)).

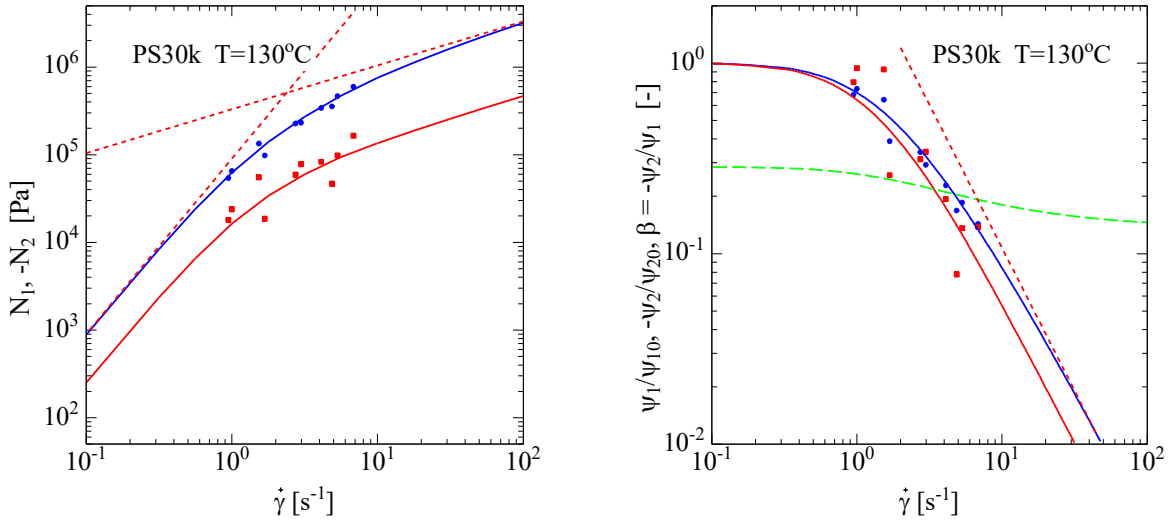

(a) (b)

Fig.9: (a) First and second normal stress difference and (b) first and second normal stress coefficient data (symbols) for PS30k as a function of shear rate $\dot{\gamma}$. Full lines are predictions of the DEIA model (Eq.(20)). The dotted lines in (a) denote a scaling of $N_1 \propto \dot{\gamma}^2$ and $N_1 \propto \dot{\gamma}^{1/2}$, respectively. Dotted line in (b) indicates $\psi_1 \propto \dot{\gamma}^{-3/2}$, long-dashed line shows $\beta = -\psi_2 / \psi_1$.

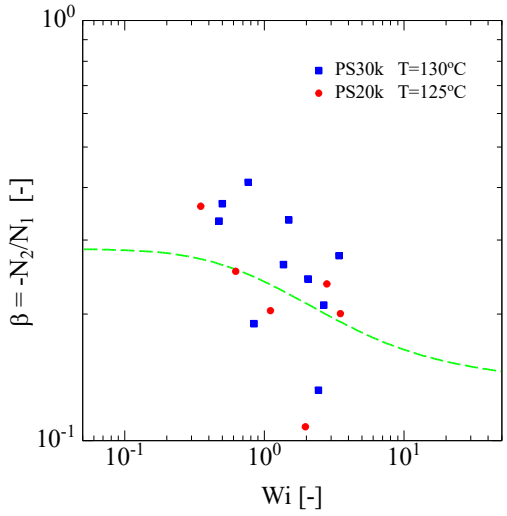

Fig.10: Ratio β of the second to the first normal stress difference data (symbols) for PS20k and PS30k as a function of Weissenberg number $Wi = \dot{\gamma}\tau_R$. Long-dashed curve is prediction of the DEIA model of Eq.(20).

CONCLUSIONS

The analysis of the shear rheology of unentangled polymer melts leads to the following conclusions:

1. The terminal relaxation regime relevant for the flow properties of unentangled polymers is determined by an inseparable combination of (entropic) Rouse and (energetic) glassy modes with different time dependencies. The smaller the radius of gyration of the macromolecule, the denser is the packing of the macromolecule, which leads to enhanced energetic intra- and inter-chain interactions. Both entropic and energetic effects determine the modulus G characterizing effective Rouse modes, which scales with molar mass M according to $G \propto M^{-3/2}$ instead of $G \propto M^{-1}$ as expected for pure entropic elasticity.

2. The steady-state nonlinear shear flow of unentangled polymers can be modeled by the Doi-Edwards Independent Alignment (DEIA) model with a relaxation time spectrum of effective Rouse modes. In steady-state shearing, chains are oriented but not stretched.

3. The DEIA model is fully characterized by effective Rouse modes with only two parameters, modulus G and Rouse time τ_R, which can be fitted to the experimentally determined shear viscosity $\eta(\dot{\gamma})$. If a reliable value of the zero-shear viscosity η_0 is available, only one fit parameter is needed, either G or τ_R. If η_0 as well as the first normal stress coefficient in the second order limit, ψ_{10}, are known, G and τ_R are identified univocally.

4. The normalized shear viscosity η/η_0, the normalized first and second normal stress coefficients, ψ_1/ψ_{10} and ψ_2/ψ_{20}, as well as the ratio $\beta = -\psi_2/\psi_1$ are universal material functions of $Wi = \dot{\gamma}\tau_R$ in agreement with available experimental evidence.

5. In start-up of shear flow, chains are initially oriented and stretched, but the stretch relaxes in steady-state shearing. Without introducing any new parameter, the transient shear viscosity $\eta^+(\dot{\gamma},t)$ can be described by the RZS model (Wagner et al. 2024), which reduces to the DEIA model in steady-state shear flow. We remark that the RZS model also describes the shear rheology of entangled polymers, albeit with a reptation–type relaxation time spectrum. The similarity of the shear rheology of unentangled versus entangled polymers has a common origin: Persistent orientation of polymer chains whether entangled or not, while initial stretch at the start-up of flow is relaxing in steady-state shearing.

Statements and Declarations

Compliance with ethical standards

Not applicable

Author contribution

MHW is the sole author of this work

Consent for publication

MHW agrees to publication

Competing interests

MHW declares no competing interests

Data availability

Data are available upon reasonable request

Funding

No funding has been received for this work

Author information

ORCID: 0000-0002-1815-7060

Acknowledgements

The author thanks Salvatore Costanzo and Katerina Peponaki for sharing the original data analyzed in this work.

REFERENCES

Colby R, Boris D, Krause W, Dou S (2007) Shear thinning of unentangled flexible polymer liquids. Rheol Acta 46: 569-575

Costanzo S (2026) Private communication

Dalne M, Costanzo S, Peponaki K, Jiang N, Alexandris S, Grizzuti N, Vlassopoulos D, Rubinstein M, Van Ruymbeke E (2025) Nonlinear Shear Rheology of Unentangled Polymer Melts. Macromolecules 58:7062−7083

Fetters LJ, Lohse DJ, Colby RH (2007) Chain Dimensions and Entanglement Spacings. In: Mark JE (ed) Physical Properties of Polymers Handbook. Springer New York, New York, NY, pp 447-454

Ianniruberto G, Marrucci G (2020) Origin of Shear Thinning in Unentangled Polystyrene Melts. Macromolecules 53: 1338-1345

Lodge AS, Wu Y-j (1971) Constitutive equations for polymer solutions derived from the bead/spring model of Rouse and Zimm. Rheol Acta 10: 539-553

Narimissa E, Schweizer T, Wagner MH (2020) A constitutive analysis of nonlinear shear flow. Rheologica Acta. DOI 10.1007/s00397-020-01215-7

Narimissa E, Wagner MH (2020) Modeling nonlinear rheology of unentangled polymer melts based on a single integral constitutive equation. Journal of Rheology 64: 129-140. DOI 10.1122/1.5128295

Ngai K (2011) Relaxation and diffusion in complex systems. Springer Science & Business Media

Ngai K, Plazek D, Deo S (1987) Physical origin of the anomalous temperature dependence of the steady-state compliance of low molecular weight polystyrene. Macromolecules 20: 3047-3054

Ngai KL, Plazek DJ (1995) Identification of Different Modes of Molecular Motion in Polymers That Cause Thermorheological Complexity. Rubber Chemistry and Technology 68: 376-434. DOI 10.5254/1.3538749

Ngai KL, Plazek DJ (2007) Temperature dependences of the viscoelastic response of polymer systemsPhysical Properties of Polymers Handbook. Springer, pp 455-478

Ngai KL, Plazek DJ, Rendell RW (1997) Some examples of possible descriptions of dynamic properties of polymers by means of the coupling model. Rheologica acta 36: 307-319

Parisi D, Costanzo S, Jeong Y, Ahn J, Chang T,,Vlassopoulos D, Halverson JD, Kremer K, Ge T, Rubinstein,M, Grest GS,,Srinin W, Grosberg AY (2021) Nonlinear Shear Rheology of Entangled Polymer Rings. Macromolecules 54: 2811−2827

Plazek DJ (1965) Temperature Dependence of the Viscoelastic Behavior of Polystyrene. The Journal of Physical Chemistry 69: 3480-3487. DOI 10.1021/j100894a039

Plazek DJ, Ngai KL (1991) Correlation of polymer segmental chain dynamics with temperature-dependent time-scale shifts. Macromolecules 24: 1222-1224. DOI 10.1021/ma00005a044

Plazek DJ, O'Rourke VM (1971) Viscoelastic behavior of low molecular weight polystyrene. Journal of Polymer Science Part A‐2: Polymer Physics 9: 209-243

Plazek DJ, Schlosser E, Schönhals A, Ngai KL (1993) Breakdown of the Rouse model for polymers near the glass transition temperature. The Journal of Chemical Physics 98: 6488-6491. DOI 10.1063/1.464788

Poh L, Narimissa E, Wagner MH (2020) Universality of steady shear flow of Rouse melts. Rheol. Acta 59: 755–763

Psevdos C, Ianniruberto G (2026) Flow-Induced Friction Reduction in Shear Flows of Unentangled Polymer Melts. Macromolecules 59: 9154−9161

Roland CM, Ngai KL, Santangelo PG, Qiu XH, Ediger MD, Plazek DJ (2001) Temperature Dependence of Segmental and Terminal Relaxation in Atactic Polypropylene Melts. Macromolecules 34: 6159-6160. DOI 10.1021/ma002121p

Santangelo P, Roland C (1998) Molecular weight dependence of fragility in polystyrene. Macromolecules 31: 4581-4585

Santangelo P, Roland C (2001) Interrupted shear flow of unentangled polystyrene melts. Journal of Rheology 45: 583-594

Stratton RA (1972) Non-Newtonian flow in polymer systems with no entanglement coupling. Macromolecules 5: 304-310

Wagner MH, Liu S, Huang Q (2024) The effect of rotationality on nonlinear shear flow of polymer melts and solutions. Rheol. Acta 63: 573–584

Winter HH, Mours M (2006) The cyber infrastructure initiative for rheology. Rheol Acta 45: 331-338